A&A, 707, C4 (2026)
https://doi.org/10.1051/0004-6361/202659136e

Astronomy & Astrophysics

Stellar angular momentum of intermediate-redshift galaxies in MUSE surveys *(Corrigendum)*

C. Muñoz López[1,⋆], D. Krajnović[1], B. Epinat[2,3], Y. Herrero-Alonso[1], T. Urrutia[1], W. Mercier[3,4], N. F. Bouché[5], L. A. Boogaard[6], T. Contini[4], L. Michel-Dansac[3,5], and I. Pessa[1]

[1] Leibniz-Institut für Astrophysik Potsdam (AIP), An der Sternwarte 16, 14482 Potsdam, Germany
[2] Canada-France-Hawaii Telescope, 65-1238 Mamalahoa Highway, Kamuela, HI 96743, USA
[3] Aix Marseille Univ., CNRS, CNES, LAM, Marseille, France
[4] Institut de Recherche en Astrophysique et Planétologie (IRAP), Université de Toulouse, CNRS, UPS, CNES, Toulouse, France
[5] Centre de Recherche Astrophysique de Lyon UMR5574, Univ. Lyon1, ENS de Lyon, CNRS, F-69230 Saint-Genis-Laval, France
[6] Max Planck Institute for Astronomy, Königstuhl 17, 69117 Heidelberg, Germany

A&A, 688, A75 (2024), https://doi.org/10.1051/0004-6361/202449758

Key words. galaxies: evolution – galaxies: formation – galaxies: kinematics and dynamics – errata, addenda

1. Introduction

This is an erratum of Muñoz López et al. (2024) addressing the miscalculated values of the spin parameter, λ_R, defined by Eq. (1) (Eq. 1 in the original publication):

$$\lambda_R \equiv \frac{\langle R \mid V \mid \rangle}{\langle R\sqrt{V^2+\sigma^2}\rangle} = \frac{\sum_{i=1}^{N} F_i R_i \mid V_i \mid}{\sum_{i=1}^{N} F_i R_i \sqrt{V_i^2+\sigma_i^2}}. \quad (1)$$

When calculating the spin parameter, the galaxy's systemic velocity was not subtracted from the mean stellar velocity (V), resulting in an inaccurate estimation of the spin parameter. The typical galaxy's systemic velocity was ∼70 km/s, which resulted in an average error of ∼15% for λ_R.

We present here the corrected values of λ_R and the updated versions of the corresponding figures (Figures 4–9 in the original publication). We also report the updated values of λ_R in column (3) of Table 1, which complements Table B.1 in the original publication.

The change in the λ_R values requires updating several plots from the original paper. Nevertheless, the main conclusions of this paper remain unchanged. The main changes are:

- For most galaxies, their λ_R values are lower than previously reported, which makes our sample more similar to galaxies in the local Universe.
- We find three slow rotators within the redshift range of the sample (instead of one).
- The trend in low-mass galaxies with high star formation rates (SFR) (located above the main sequence in the stellar mass-SFR diagram) toward lower spin parameters is now more pronounced and resembles that seen in the $z = 0$ galaxy population.

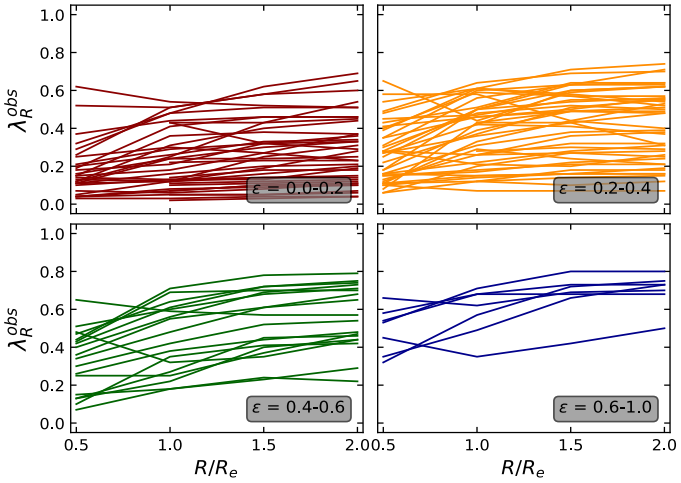

Fig. 1. Updated observed stellar angular momentum profile for the sample galaxy for different aperture radii (0.5, 1.0, 1.5, and $2\,R_e$) relative to the effective radius. The values are not seeing-corrected. The colours indicate the galaxy ellipticity ϵ, which is also indicated in each panel. This figure corresponds to the updated version of Figure 4 in Muñoz López et al. (2024).

2. Updated figures

2.1. Observed spin parameter

In Figure 1 we present the updated version of Figure 4 from the original publication. The main consequence of removing the galaxy's systematic velocity when computing the spin parameter is the resulting lower values of λ_R for all the galaxy's ellipticity bins shown in the figure. Our main conclusions – that the sample is dominated by round galaxies and that the observed radial λ_R profiles do not change dramatically between 0.5 and $2\,R_e$ – remain unaltered.

⋆ Corresponding author: cmunoz@aip.de

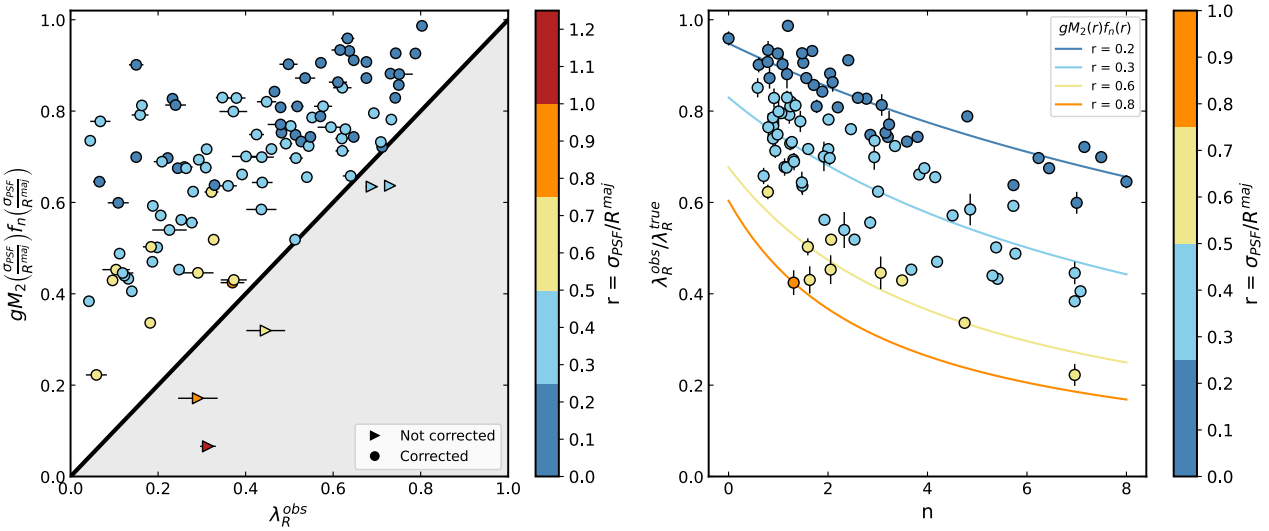

Fig. 2. Updated corrections for the spin parameter in the galaxy sample. Both panels (*left* and *right*) are colour-coded by the ratio (r) of the galaxy's angular size to the PSF, given by the major-axis $R^{\rm maj}$ and $\sigma_{\rm PSF}$, respectively. The ratio r is a parameter that quantifies how well-resolved a galaxy is. *Left*: Generalized Moffat and empirical f_n functions as correction indicators from Graham et al. (2018) and their dependence on the observed (measured) stellar spin parameter, the galaxy angular size, and the width of the PSF. The shaded part of the plot indicates the region where the galaxy spin parameter correction is not physical, leading to $\lambda_R^{\rm true} > 1$. Thus, for galaxies with $r > 1$, no seeing correction is applied. Triangles and circles indicate uncorrected and corrected galaxies, respectively. Triangles can be interpreted as lower limit values. *Right*: Comparison between the observed and intrinsic angular momentum as a function of the galaxy Sérsic index for the corrected galaxies. The solid lines indicate the predicted behaviour of the corrections as a function of the Sérsic index for the mean r values of the respective subsets. This figure corresponds to the updated version of Figure 5 in Muñoz López et al. (2024).

2.2. Atmospheric seeing corrections for λ_R

Figure 2 shows the updated version of Figure 5 in the original paper. As most of the observed stellar angular momentum values in the sample decreased (i.e. lower $\lambda_{\rm R}^{\rm obs}$ values), we corrected additional galaxies for the point spread function (PSF) effects using

$$\lambda_{\rm R}^{\rm obs} / gM_2\left(\frac{\sigma_{\rm PSF}}{R^{\rm maj}}\right) f_n\left(\frac{\sigma_{\rm PSF}}{R^{\rm maj}}\right) = \lambda_{\rm R}^{\rm true}. \quad (2)$$

In Equation (2), the parameters referring to the galaxy's angular size and the PSF, given by the major-axis $R^{\rm maj}$ and $\sigma_{\rm PSF}$, remain unchanged. Therefore, given the new values of λ_R, more galaxies have parameter combinations where $\lambda_{\rm R}^{\rm obs}$, the gM_2, and the f_n functions result in $\lambda_{\rm R}^{\rm true} \leq 1$. This is manifested by the correction of 101 out of 106 galaxies (compared to 80 in Muñoz López et al. 2024).

2.3. Stellar spin parameter

In Figure 3 we present the updated version of Figure 6 in Muñoz López et al. (2024). Our original results remain unchanged with the following exceptions:

- There is a decrease in the number of galaxies with high angular momentum.
- The fraction of galaxies with $\lambda_R \geq 0.8$ diminishes.
- The fraction of galaxies with $\lambda_R < 0.8$ increases.
- Additionally, galaxy 73, galaxy 51, and galaxy 71 are now classified as slow rotators. All three galaxies have spin parameters corrected for atmospheric seeing. These systems account for a total of three slow-rotating galaxies in the sample.

Galaxies 51 and 71 are at $z = 0.62$ and $z = 0.69$, respectively, with low star formation rates: $\log_{10}({\rm SFR}) \approx -0.59\,{\rm M}_\odot\,{\rm yr}^{-1}$ and $\log_{10}({\rm SFR}) \approx -1.25\,{\rm M}_\odot\,{\rm yr}^{-1}$. Both galaxies are massive with stellar masses of $10^{11.4}\,{\rm M}_\odot$ and $10^{10.5}\,{\rm M}_\odot$, respectively.

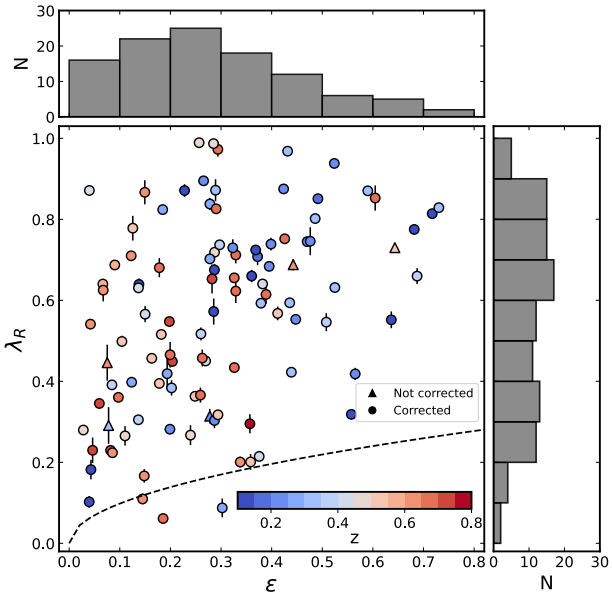

Fig. 3. Updated λ_R as a function of ellipticity, colour-coded by redshift, for the 106 sample galaxies, with histograms. The circles indicate galaxies where the spin parameter was corrected for atmospheric seeing; the value corresponds to the intrinsic stellar angular momentum ($\lambda_R^{\rm true}$). The triangles mark galaxies where corrections could not be applied, showing measured values ($\lambda_R^{\rm obs}$) that can be considered lower limits. The dashed black line denotes the threshold between slow and fast rotators, given by $0.31 \times \sqrt{\epsilon}$ (Emsellem et al. 2011). This figure corresponds to the updated version of Figure 6 in Muñoz López et al. (2024).

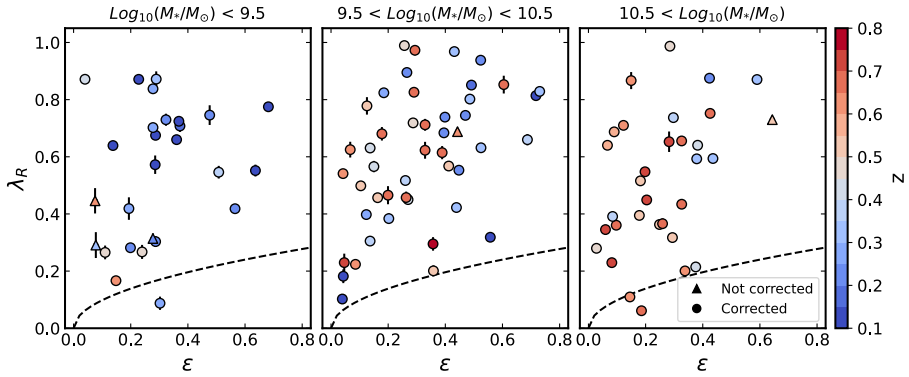

Fig. 4. Updated λ_R as a function of galaxy ellipticity, colour-coded by redshift, for the three different mass bins indicated in the top part of each panel. The dashed black lines denote the threshold between slow and fast rotators. Uncorrected and corrected λ_R values are indicated by triangles and circles, respectively. This figure corresponds to the updated version of Figure 7 in Muñoz López et al. (2024).

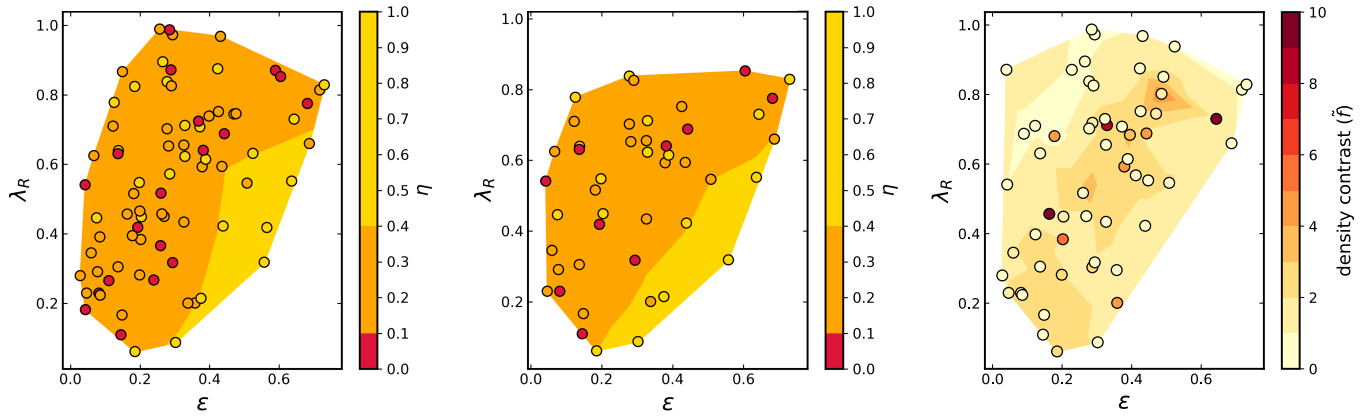

Fig. 5. Updated λ_R–ϵ plane, colour-coded by two different environmental indicators. The background in all panels shows a LOESS-smoothed version of the dots above. *Left*: η indicator computed using the FoF algorithm for all galaxies detected in groups. *Middle*: η indicator computed using the FoF algorithm for galaxies detected in groups with ten members or fewer. *Right*: Density contrast ($\hat{f}$) estimator obtained from the Voronoi tessellation method. This figure corresponds to the updated version of Figure 8 in Muñoz López et al. (2024).

Figure 4 is the updated version of Figure 7 in the original publication. We observed that the two additional slow rotators (galaxies 51 and 71) lie in the most massive stellar mass bin.

2.4. Environment indicators

We present the updated version of Figure 8 (Muñoz López et al. 2024) in Figure 5. In the middle panel of Figure 5, no galaxies have $\lambda_R > 0.8$, indicating that all galaxies with $\lambda_R < 0.8$ belong to groups with more than ten members. Thus, group galaxies with $\lambda_R > 0.8$ belong to less massive groups (fewer than ten members), as observed in the left panel.

Due to the changes in λ_R, more galaxies now fall within the parameter range where the PSF correction is stronger (right panel of Figure 5). However, the point distributions in the original and updated figure are similar. Even so, our main conclusion regarding stellar kinematics and sample environment remains unchanged: the relatively low-density environment of the galaxies in this work does not strongly influence λ_R.

2.5. Stellar mass, star formation rate, and spin parameter

Figure 6 is the updated version of Figure 9 (Muñoz López et al. 2024). Galaxies with low star formation rates have lower values of angular momentum, which resemble the population of slow rotators at $z = 0$. Furthermore, the new λ_R values show

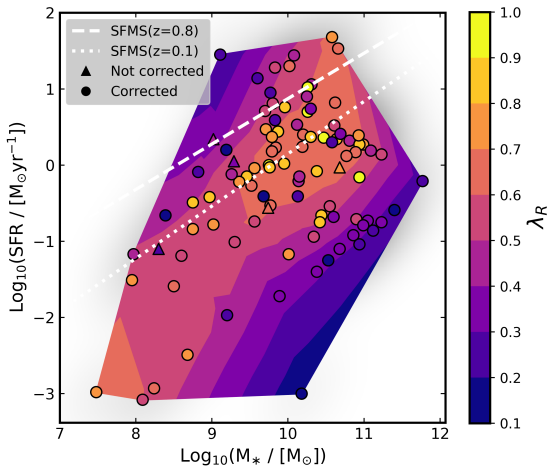

Fig. 6. Updated star formation rate as a function of stellar mass colour-coded by λ_R. The grey-shaded region in the background corresponds to the 3D-HST sample measurement. The dotted and dashed white lines indicate the star formation main sequence for Universe ages of 12.4 Gyr ($z = 0.1$) and 6.8 Gyr ($z = 0.8$), respectively, from Eq. (1) of Whitaker et al. (2012). The colour map shows a LOESS-smoothed version of the markers on top. The dots and triangles represent seeing-corrected and uncorrected values, respectively. This figure corresponds to the updated version of Figure 9 in Muñoz López et al. (2024).

Table 1. Updated spin parameters for the galaxy sample.

N	ID	λ_R	N	ID	λ_R
1	17979	• 0.593 ± 0.004	56	23102	• 0.360 ± 0.003
2	18117	• 0.594 ± 0.004	57	20254	• 0.987 ± 0.001
3	16844	• 0.434 ± 0.007	58	20671	• 0.680 ± 0.024
4	11752	• 0.814 ± 0.003	59	29048	• 0.871 ± 0.012
5	7336	• 0.384 ± 0.019	60	21890	• 0.708 ± 0.021
6	20094	• 0.281 ± 0.010	61	25172	• 0.875 ± 0.005
7	14733	• 0.687 ± 0.010	62	30133	• 0.968 ± 0.007
8	17138	• 0.719 ± 0.010	63	30082	• 0.702 ± 0.011
9	17034	• 0.684 ± 0.007	64	26377	• 0.631 ± 0.008
10	15773	• 0.318 ± 0.004	65	25909	• 0.265 ± 0.024
11	17928	• 0.457 ± 0.012	66	22942	• 0.224 ± 0.006
12	16635	• 0.553 ± 0.011	67	28995	• 0.295 ± 0.027
13	19745	↑ 0.314 ± 0.018	68	27438	• 0.775 ± 0.012
14	27563	• 0.517 ± 0.016	69	29238	↑ 0.688 ± 0.014
15	28410	• 0.422 ± 0.011	70	29794	• 0.541 ± 0.004
16	19146	• 0.895 ± 0.003	71	27965	• 0.109 ± 0.013
17	28888	• 0.938 ± 0.005	72	28445	• 0.166 ± 0.017
18	32156	• 0.305 ± 0.007	73	29861	• 0.087 ± 0.023
19	33471	• 0.972 ± 0.018	74	2957	• 0.280 ± 0.009
20	26491	• 0.566 ± 0.020	75	3487	• 0.615 ± 0.023
21	29723	• 0.660 ± 0.020	76	4148	• 0.391 ± 0.005
22	31246	• 0.303 ± 0.019	77	1996	• 0.215 ± 0.005
23	24878	• 0.230 ± 0.004	78	902	• 0.640 ± 0.004
24	17223	• 0.752 ± 0.005	79	4596	• 0.449 ± 0.006
25	10176	• 0.395 ± 0.008	80	4638	• 0.872 ± 0.027
26	8813	• 0.363 ± 0.006	81	4077	• 0.640 ± 0.008
27	31463	• 0.546 ± 0.022	82	5116	• 0.551 ± 0.021
28	32648	↑ 0.730 ± 0.005	83	901	• 0.398 ± 0.009
29	27247	• 0.655 ± 0.009	84	3165	• 0.802 ± 0.006
30	26402	• 0.548 ± 0.005	85	3637	• 0.745 ± 0.010
31	26138	• 0.345 ± 0.004	86	3880	• 0.851 ± 0.006
32	30082	• 0.838 ± 0.015	87	14034	• 0.737 ± 0.003
33	17361	• 0.201 ± 0.019	88	27564	• 0.852 ± 0.031
34	20356	• 0.829 ± 0.009	89	29169	• 0.746 ± 0.034
35	20898	• 0.568 ± 0.017	90	27535	• 0.419 ± 0.040
36	36482	• 0.498 ± 0.014	91	25053	• 0.201 ± 0.013
37	30918	• 0.632 ± 0.010	92	28356	• 0.625 ± 0.028
38	31801	• 0.639 ± 0.015	93	25487	• 0.267 ± 0.025
39	32778	• 0.572 ± 0.032	94	26233	↑ 0.446 ± 0.044
40	32762	• 0.871 ± 0.016	95	25652	↑ 0.291 ± 0.045
41	21978	• 0.450 ± 0.012	96	25884	• 0.366 ± 0.019
42	25622	• 0.739 ± 0.016	97	9612	• 0.724 ± 0.010
43	28098	• 0.870 ± 0.003	98	12252	• 0.102 ± 0.014
44	21832	• 0.318 ± 0.005	99	36313	• 0.182 ± 0.024
45	16742	• 0.990 ± 0.008	100	10195	• 0.457 ± 0.021
46	32855	• 0.675 ± 0.015	101	20331	• 0.653 ± 0.036
47	46386	• 0.824 ± 0.004	102	9754	• 0.466 ± 0.032
48	6203	• 0.516 ± 0.004	103	17534	• 0.418 ± 0.015
49	11536	• 0.778 ± 0.031	104	26322	• 0.623 ± 0.030
50	23802	• 0.826 ± 0.003	105	35579	• 0.867 ± 0.030
51	24622	• 0.061 ± 0.009	106	3181	• 0.660 ± 0.015
52	26322	• 0.712 ± 0.020			
53	29845	• 0.710 ± 0.006			
54	25592	• 0.230 ± 0.031			
55	26639	• 0.730 ± 0.021			

Notes. Column N: galaxy index; column ID: 3D-HST galaxy unique identifier within a given field; column λ_R: updated galaxy stellar angular momentum measured for the selected aperture. The arrows (↑) correspond to galaxies where the seeing correction was not applied and thus indicate measured values. The filled dots (•) indicate galaxies with corrected values. Column (3) is an updated version of column (15) from Table B.1 in Muñoz López et al. (2024).

with greater significance that low-mass galaxies above the main sequence likely have low stellar angular momentum, as seen in Wang et al. (2020) for $z = 0$ galaxies. Figure 6 of the original paper showed only tentative hints that this might be the case, whereas the new values provide stronger evidence.

3. Summary of updated results

In conclusion, we summarize the changes of our study when updating the spin parameter λ_R:

- Most of the updated stellar angular momentum values decreased because we removed the galaxy's systematic velocity when computing the spin parameter λ_R.
- As a consequence, more galaxies can now be corrected for atmospheric seeing. Compared to 80 out of 106 systems previously, we can now PSF-correct 101 galaxies in total.
- Our sample contains three slow rotators. Two additional galaxies at $z > 0.6$ are slow-rotating (Galaxies 51 and 71), which share the main properties of the slow rotators in the local Universe.
- Our conclusions regarding λ_R and the environment remain unchanged.
- The new λ_R values show greater similarity between intermediate-redshift galaxies and the local population: low-angular-momentum galaxies are found below the star-forming main sequence, and above it for low-mass galaxies.

References

Cappellari, M. 2016, ARA&A, 54, 597
Emsellem, E., Cappellari, M., Krajnović, D., et al. 2011, MNRAS, 414, 888
Graham, M. T., Cappellari, M., Li, H., et al. 2018, MNRAS, 477, 4711
Muñoz López, C., Krajnović, D., Epinat, B., et al. 2024, A&A, 688, A75
Wang, B., Cappellari, M., Peng, Y., et al. 2020, MNRAS, 495, 1958
Whitaker, K. E., van Dokkum, P. G., Brammer, G., et al. 2012, ApJ, 754, L29